JOURNAL OF MATERIALS SCIENCE: MATERIALS IN MEDICINE 3 (1992) 54–58

Phase transformation behaviour of a low carat gold alloy for porcelain bonding during continuous heating

K. HISATSUNE, Y. TANAKA, T. TANI, K. UDOH, K. YASUDA
Department of Dental Materials Science, Nagasaki University School of Dentistry, Nagasaki 852, Japan

The phase transformation associated with hardening in a low carat gold alloy for porcelain bonding during continuous heating was studied by resistivity measurements, hardness tests, X-ray diffraction and scanning and transmission electron microscopies. A short-range order structure, based on Au–Pd, was produced at a lower temperature. At an elevated temperature, two types of precipitation were observed. One is a nodular reaction consisting of an $L1_2$ ordered structure based on Pd_3Sn and a disordered FCC structure at grain boundary. The other is a formation of spherical $L1_2$ ordered precipitates based on Pd_3Sn within the grain followed by Ostwald ripening. A fine dispersed precipitate of the latter contributed to the remarkable hardening.

1. Introduction

In the past decade, many kinds of alloys for porcelain bonding have been developed. It is well known that most of these alloys demonstrate age-hardening because of small additions such as In, Sn or Fe [1–12]. However, the hardening reactions themselves have been elucidated imperfectly. As these alloys do not contain any copper, because of producing a greenish colour in the porcelain, the formation of CuAuI cannot be expected for the hardening. In the gold-base alloys, Smith *et al.* [6] and Fuys *et al.* [7] speculated a precipitation of an ordered face-centred cubic (FCC) structure $FePt_3$. Recently, German [10] detected an ordered face-centred tetragonal (FCT) structure phase $PtFe_{0.6}Co_{0.3}$ as a hardening reaction product. On the other hand, only the existence of an FCT structure based on Pd_3In in the palladium-base alloy [12] and of age-hardening in the low carat gold alloys [9, 11] have been reported. The phase transformation behaviour in these alloys has been unclear.

The aim of the present study was to clarify the phase transformation behaviour in a low carat gold alloy for porcelain bonding during continuous heating by using electrical resistivity measurements, hardness tests, X-ray diffraction (XRD), scanning and transmission electron microscopies (SEM and TEM).

2. Material and methods

The alloy used in the present study was a low carat gold alloy for porcelain bonding with composition 45 wt % Au–32 wt % Pd–19 wt % X (Neydium, The J. M. Ney Co., USA). The symbol X denotes the constituents not given by the manufacturer. It was revealed by an energy dispersive X-ray analysis in the present study that they were Ag and Sn.

Sheets of 0.5 or 0.1 mm thickness were prepared by alternate rolling and annealing for hardness tests and other experiments, respectively. These specimens were solution-treated at 1000 °C for 30 min and then quenched into ice brine. Anisothermal annealing was subsequently carried out at a heating rate of 0.25, 0.5, 1, or 10 °C min^{-1} from room temperature to 1000 °C *in vacuo*. The hardness tests were made by using a diamond pyramid hardness indenter with a 200 g load. Each hardness value quoted is the average of five indentations. The electrical resistivity measurements were made by using a potentiometric method. The structural changes were examined with XRD, SEM and TEM. Specimens for the SEM observations were prepared by using a standard metallographic technique, with final etching achieved with a freshly prepared aqueous solution of 10% potassium cyanide and 10% ammonium persulphate. For the TEM study, discs of 3 mm diameter were punched out and subjected to appropriate annealing. They were electrothinned by a double-jet technique in a solution of 35 g of CrO_3, 200 ml of CH_3COOH and 10 ml of H_2O. The electron microscopes used were operated at 20 and 200 kV, respectively. The XRD study was carried out on the filed and appropriately heat-treated powder specimens by using nickel-filtered CuK_α radiation.

3. Results and discussion

3.1. Electrical resistivity changes

Fig. 1a shows an anisothermal annealing curve of

0022–2461/92 $03.00 + .12

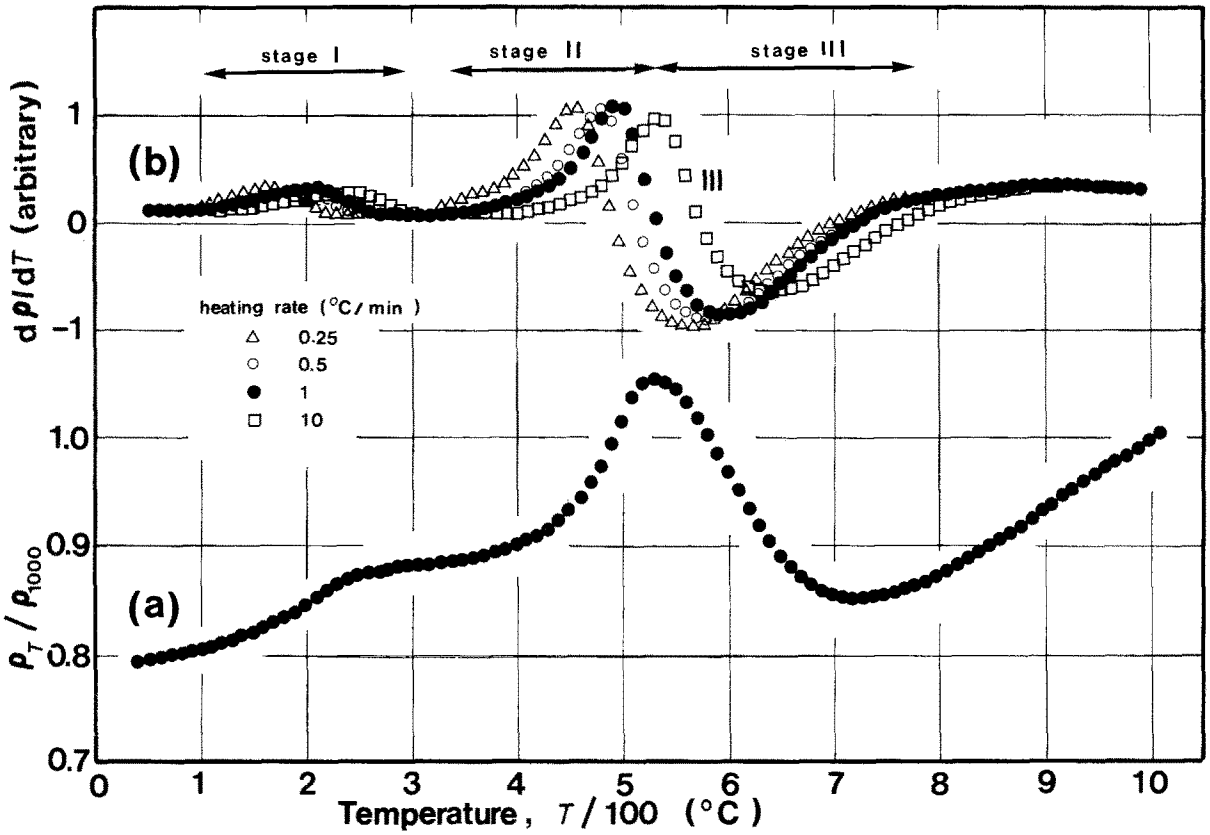

Figure 1 Variation of electrical resistivity and its temperature derivatives during continuous heating with temperature.

electrical resistivity (ρ) at a heating rate of 1°C min^{-1}. Normalized resistivity (ρ_T/ρ_{1000}) is a ratio of the resistivity at each measured temperature (T°C) and that at a solution-treated temperature (1000 °C). Fig. 1b shows the temperature derivative curves. It is noted that the variation of them clearly indicates the heating rate dependence. These changes seem to be attributed to some phase transformations. As can be seen in Fig. 1b, four kinds of phase transformations are implied. Stages I and II indicate increases of resistivity, while stage III indicates a decrease. The change of stage IV was very small and not clear in the figure. It is thought that this stage corresponds to a reaction to an equilibrium single phase. Our preliminary work revealed that the quenching after solution treatments at 950 °C and 1000 °C had produced two phases and a single phase, respectively. Therefore, it is expected that a phase transformation temperature exists between 950 and 1000 °C.

If the amount of reaction rate can be proportional to the change of resistivity, the reaction rate may correspond to the $d\rho/dT$ value. As can be seen in Fig. 1b, the reaction rate of each stage depends strongly on the heating rate. It is well known that there is a relationship, as shown below by the Kissinger's equation [13], between the activation energy and the rate dependence,

$$d(\ln \Phi T_m^{-2})/dT_m^{-1} = -E/R$$

where Φ is the heating rate, T_m the temperature at which the reaction rate attained a maximum value, E the activation energy and R the gas constant. Applying Kissinger's equation to this rate dependence,

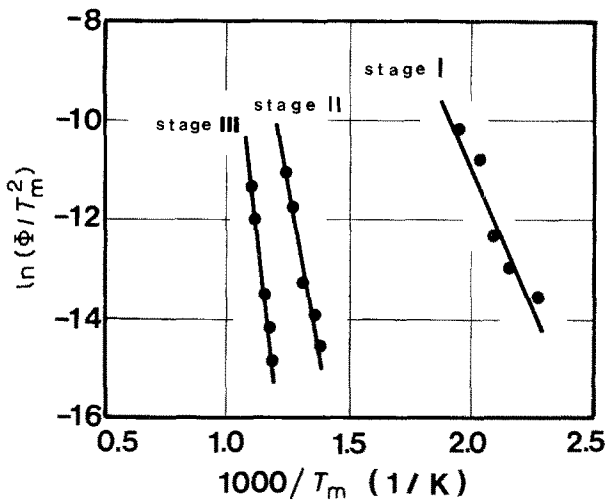

Figure 2 Application of Kissinger's equation for each stage.

straight lines were obtained, as shown in Fig. 2. The activation energies are then calculated from the slope of each straight line. The apparent activation energies for stages I, II and III were 20.6, 34.7 and 75.4 kcal mol^{-1}, respectively.

3.2. Age-hardening behaviour

Fig. 3 shows variation of hardness with temperature during continuous heating at a rate of 1 °C min^{-1}. The hardness begins to increase from about 400 °C and attains a peak at about 700 °C. Thereafter, softening occurs with elevating the temperature. The temperature region that produced remarkable hardening corresponds to that of stage III. Comparing Fig. 3 with

Fig. 1 at this temperature, it is thought that the hardening is proportional to the output of the resistivity change in stage III.

3.3. Ageing reactions

Fig. 4 shows variation of the 422 reflection of the specimen during continuous heating at a rate of $1\,^{\circ}C\,min^{-1}$. The XRD examinations could not detect any new phase at stages I and II up to 500 °C, as shown in Fig. 4a–c. As can be seen in Fig. 1, stage I was accompanied by a small increase of resistivity, which implies a formation of short-range order (SRO) or clustering. Fig. 5 shows a selected-area electron diffraction (SAED) pattern with [0 0 1] incidence of a specimen heated up to 200 °C at a rate of $1\,^{\circ}C\,min^{-1}$. The diffuse scattering due to SRO as exemplified by Ohshima *et al.* [14] in Cu–Pd alloys was observed at the superlattice spot positions. An SRO based on Au–Pd system is anticipated from the constitutional elements, as Logie *et al.* [15] and Copeland *et al.* [16] have reported the evidence in binary Au–Pd alloys.

The specimen solution-treated at 1000 °C was a single phase (α_0), having an FCC structure with a lattice constant of $a_{422} = 4.004$ Å. Note that there is a broad and weak peak in both Fig. 4d and e, as shown by the arrows. This reaction corresponds to that of stage III from the temperature region. Furthermore, the intensity increased with temperature, while α_0 decreased and disappeared at 850 °C, as can be seen in Fig. 4f. However, another peak appeared near 142.5 of diffraction angle. After all, two phases ($\alpha + \beta$) were detected at 850 °C. These were identified as an FCC structure (α) with $a_{422} = 4.006$ Å and an ordered FCC structure (β) with $a_{422} = 3.984$ Å. It is thought that stages II and III correspond to a reaction of $\alpha_0 \rightarrow \alpha + \beta$.

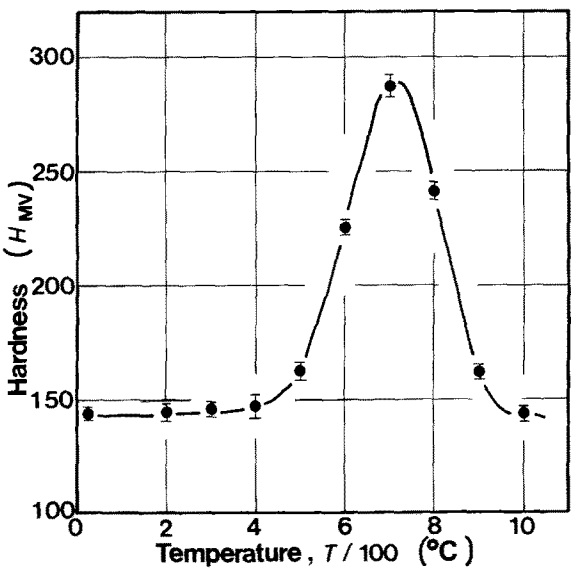

Figure 3 Variation of hardness with temperature during a continuous heating at a rate of $1\,^{\circ}C\,min^{-1}$.

Fig. 6 shows SEM images of the specimen heated up to 570 °C (a) and 720 °C (b, c) at a rate of $1\,^{\circ}C\,min^{-1}$ and quenched. The former indicated fine dispersed precipitates within grains and nodules from grain boundaries. With increasing temperature, both microstructures tended to grow, as seen in Fig. 6b. An increase of nodular spacing was observed as if the grain boundary products were consumed by the grain interior reaction. Fig. 6c is a higher magnification of the grain interior in Fig. 6b. The precipitates seem to grow up as a specific shape.

Fig. 7 shows the results of the TEM observations in stages II and III. Fig. 7a, b and d show SAED patterns with [0 0 1] incidence of specimens heated up to 500 °C, 600 °C and 700 °C, respectively. The SAED patterns indicate that a new phase with an ordered FCC structure ($L1_2$) is produced in grain interior. The new phase may correspond to the β phase, which was detected by the XRD study mentioned above. From

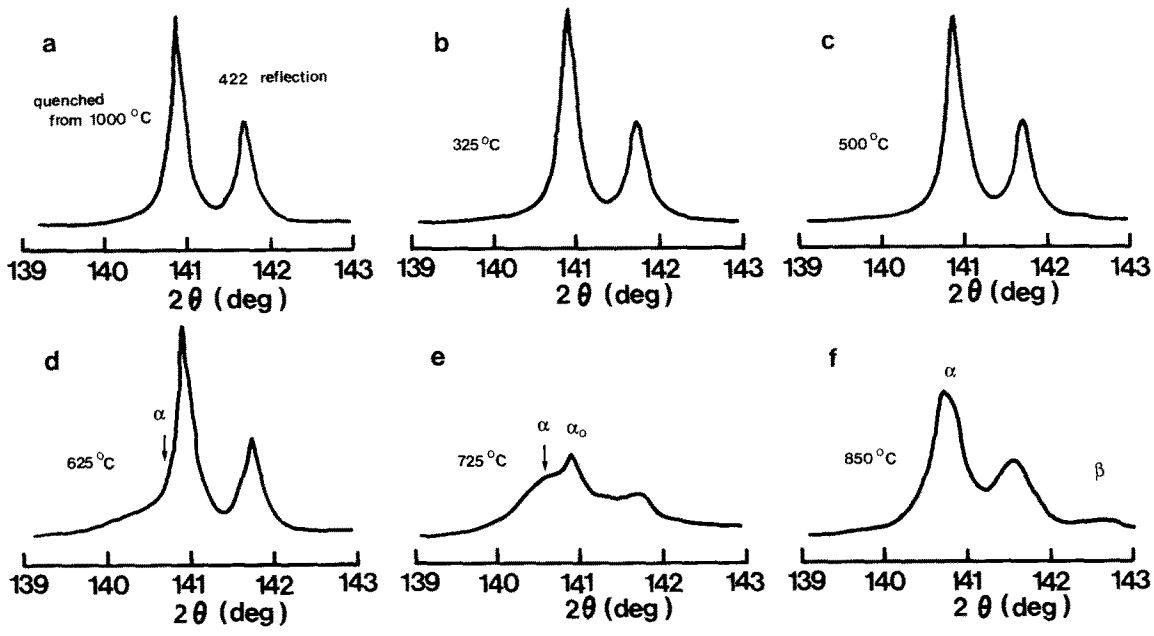

Figure 4 Variation of the 422 reflection of the specimen during continuous heating at a rate of $1\,^{\circ}C\,min^{-1}$.

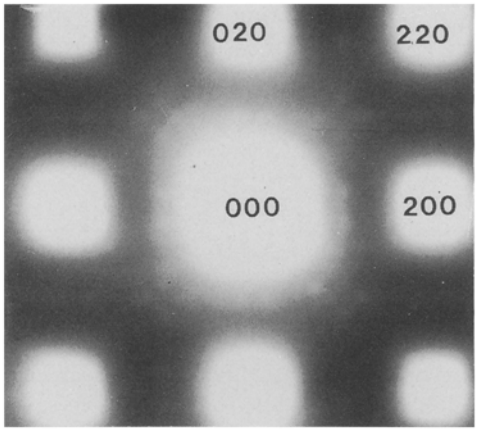

Figure 5 SAED pattern of a specimen heated up to 200 °C at a rate of 1 °C min^{-1}.

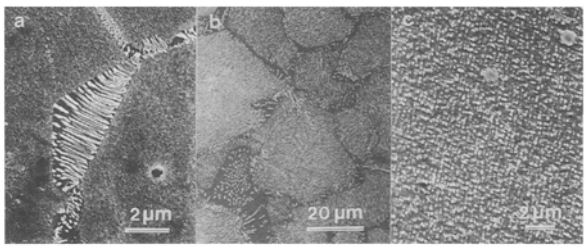

Figure 6 SEM images of the specimen heated up to (a) 570 °C and (b, c) 720 °C at a rate of 1 °C min^{-1} and quenched.

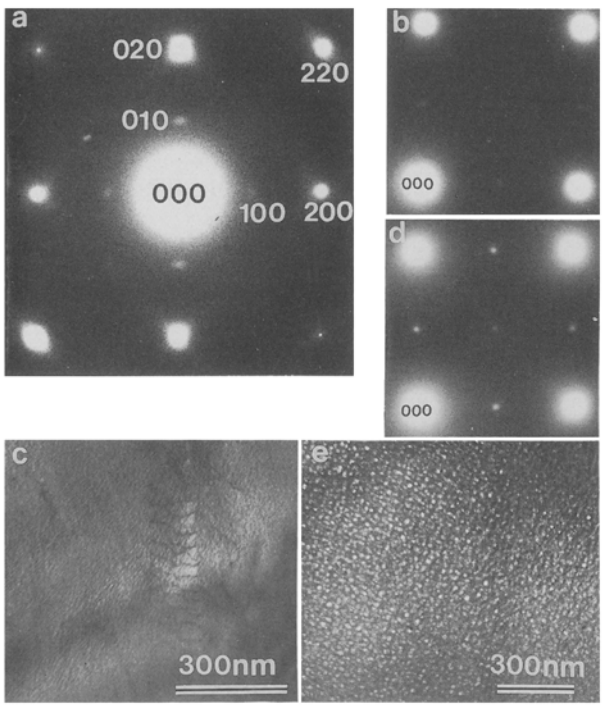

Figure 7 SAED patterns with [0 0 1] incidence and the 100 DF images of the specimen heated up to (a) 500 °C, (b, c) 600 °C and (d, e) 700 °C at a rate of 1 °C min^{-1} and quenched.

the constitutional elements, we can speculate a formation of the ordered FCC phase based on Pd_3Sn [17]. The intensity of the superlattice spots increased with temperature. The 100 DF images shown in Fig. 7c and

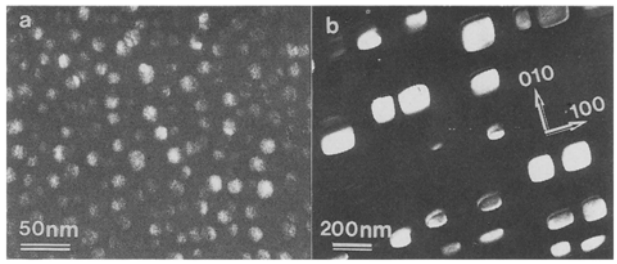

Figure 8 The 100 DF images of the specimen heated up to (a) 700 °C at a rate of 1 °C min^{-1} and then annealed at 700 °C for 7 days.

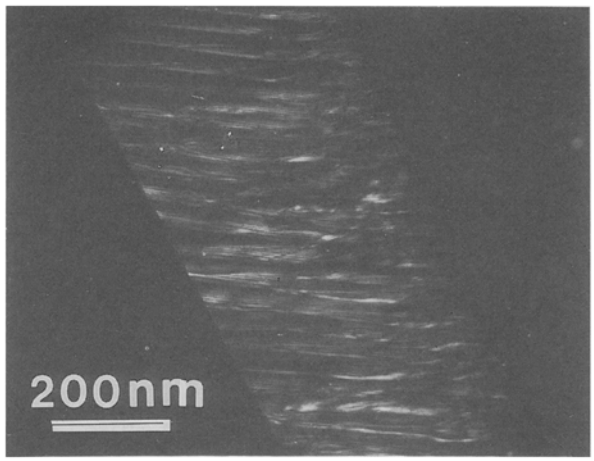

Figure 9 The 100 DF image of a specimen heated up to 500 °C at a rate of 1 °C min^{-1} and quenched.

e, revealed the growth of the $L1_2$ ordered phase. Fig. 8a shows the 100 DF image of a specimen heated up to 700 °C. The precipitates looked like spheres of about 14 nm in diameter. From the SAED pattern in Fig. 7d, it is anticipated that the precipitates have a coherency with the matrix. Therefore, this coherency strain should be produced in the specimen. We obtained a hardness peak at this condition as seen in Fig. 3. At temperatures higher than 700 °C, the hardness decreased. Fig. 8b shows the 100 DF image of a specimen aged at 700 °C for 7 days. Cuboidal precipitates 170 nm long were observed. It is obvious that the precipitates occurred with rapid growth, suggesting Ostwald ripening. The precipitates have a clear boundary on the (1 0 0) plane with the matrix. The introduction of the boundary between the precipitate and the matrix in the grain interior may produce an annihilation of the coherency strain and result in the softening. In practice, we obtained a hardness value of $H_V = 204$ in the specimen aged at 700 °C for 7 days. This reaction (stage III′), which sould be distinguished from stage III, could not be detected in the resistivity in Fig. 1.

Fig. 9 shows a 100 DF image near a grain boundary of a specimen heated up to 500 °C and quenched. The image revealed that the nodule involves the same $L1_2$ phase as detected within the grain above. The corresponding SAED pattern failed to confirm the existence of the α phase, because the difference of the lattice constant between the β and the α phases is very small.

As mentioned, in the present alloy, the hardening due to the precipitation of an ordered FCC with a structure similar to the matrix must be as favourable for porcelain metal as for the gold-base alloys [6, 7]. The softening due to Ostwald ripening may be produced during firing cycles.

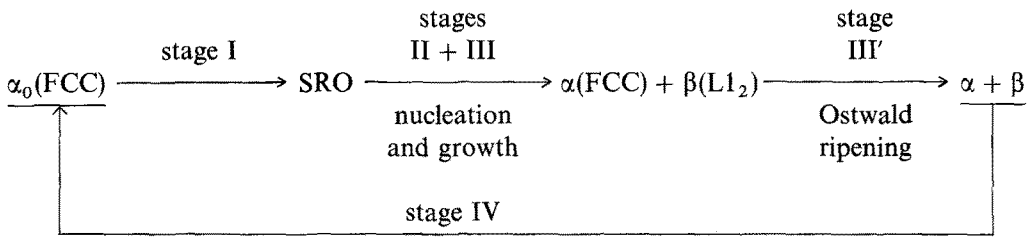

3.4. Elementary process for each stage

From the rate dependence in Fig. 2, an activation energy of 20.6 kcal mol^{-1} was obtained for stage I. An SRO associated with Au–Pd system was speculated. The energy is close to the migration energy of vacancies in pure gold, which has been estimated by Schüle *et al.* [18] and Takamura [19]. The migration of gold by means of vacancies may result in a formation of the SRO. It is very well known that excess vacancies introduced by quenching play an important role in phase transformation. Hisatsune [20] has reported a contribution of excess vacancies on the ordering in a CuPt alloy during continuous heating. Cheng *et al.* [21] and Kinoshita *et al.* [22] have shown by a method of statistical thermodynamics that the development of SRO reduces the vacancy concentration. It is thought that the excess vacancies contribute to the formation of the SRO in the present alloy.

In stage II, the resistivity attained a peak and the TEM results revealed spherical precipitates with an $L1_2$ structure. Mott [23] proposed that the peak value of the resistivity occurs when the precipitated particles attain the size for which the scattering of electrons is a maximum. On this basis, the increase and the peak in resistivity observed in stage II suggest a process to the critical size of the precipitates. As mentioned above, we speculated an $L1_2$ ordered phase based on Pd_3Sn as precipitates. Thus the migration of Pd atoms is needed for stage II. An activation energy of 34.7 kcal mol^{-1} was obtained for this stage. This value is close to a half of that for the self-diffusion of Pd [24].

Stage III may not be distinguished from stage II because of the same reaction. However, it is obvious that this stage resulted in remarkable hardening. For this stage, an activation energy of 75.4 kcal mol^{-1} was obtained. This value is close to that for the self-diffusion of Pd [24]. If it can be assumed that excess vacancies introduced by quenching are annihilated until stage II during heating, only the thermal vacancies should be effective for stage III.

4. Conclusion

Phase transformation of a low carat gold alloy for porcelain bonding during continuous heating was studied by resistivity measurements, hardness tests, XRD, SEM and TEM. The precipitation reactions are summarized as follows:

The activation energies for stages I, II and III were 20.6, 34.7, 75.4 kcal mol^{-1}, respectively. Stages (II + III) contributed to the remarkable hardening and stage III' produced the remarkable softening.

References

1. V. W. GODECKE, *Siebert-Festschrift* (1931) p. 100.
2. V. T. THIN, MSc thesis, Indiana University, Indiana (1962).
3. W. J. O'BRIEN, J. E. KRING and G. RYGE, *J. Prosth. Dent.* **14** (1964) 955.
4. W. J. O'BRIEN, K. F. LEINFELDER, C. W. FAIRHURST and G. RYGE, *J. Dent. Res.* **43** (1964) 927.
5. K. F. LEINFELDER, W. J. O'BRIEN, G. RYGE and C. W. FAIRHURST, *J. Dent. Res.* **45** (1966) 392.
6. D. L. SMITH, A. P. BURNETT, M. S. BROOKS and D. H. ANTHONY, *J. Dent. Res.* **49** (1970) 283.
7. R. A. FUYS, C. W. FAIRHURST and W. J. O'BRIEN, *J. Biomed. Mater. Res.* **7** (1973) 471.
8. F. R. SIMS, Jr, R. N. BLUMENTHAL and W. J. O'BRIEN, *J. Biomed. Mater. Res.* **7** (1973) 497.
9. E. F. HUGET, N. DVIVEDI and H. E. COSNER, Jr, *J. Prosth. Dent.* **36** (1976) 58.
10. R. M. GERMAN, *J. Dent. Res.* **59** (1980) 1960.
11. S. G. VERMILYEA, E. F. HUGET and J. M. VILCA, *J. Prosth. Dent.* **44** (1980) 294.
12. K. HISATSUNE, K. UDOH, M. NAKAGAWA and K. YASUDA, *Dent. Mater. J.* **6** (1987) 54.
13. H. E. KISSINGER, *Anal. Chem.* **29** (1957) 1702.
14. K. OHSHIMA and D. WATANABE, *Acta Crystallogr.* **A29** (1973) 520.
15. H. J. LOGIE, J. JACKSON, J. C. ANDERSON and F. R. N. HABARRO, *Acta Metall.* **9** (1961) 707.
16. W. D. COPELAND and M. E. NICHOLSON, *Acta Metall.* **12** (1964) 321.
17. J. REZEK, M. SCHLESINGER and O. T. WOO, *Mater. Sci. Engng* **18** (1975) 163.
18. W. SCHULE, A. SEEGER, F. RAMSTEINER, D. SCHULEMACHER and K. KING, *Z. Naturforsch* **15a** (1961) 323.
19. J. TAKAMURA, *Acta Metall.* **9** (1961) 547.
20. K. HISATSUNE, *J. Jpn Inst. Metals* **42** (1978) 118.
21. G. Y. CHENG, P. P. WYNBLATT and J. E. DORN, *Acta Metall.* **15** (1967) 1035.
22. C. KINOSHITA and T. EGUCHI, *Acta Metall.* **20** (1972) 45.
23. N. F. MOTT, *J. Inst. Metals* **60** (1937) 267.
24. S. KODA, in "Introduction to metal physics" (Corona Publishing Co., Tokyo, 1979) p. 120.

Received 19 October
and accepted 21 December 1990